Supplement for the manuscript—"Combining the U-Net model and a Multi-textRG algorithm for fine SAR ice-water classification"

Yan Sun[1, 2], Shaoyin Wang[1, 2], Xiao Cheng[1, 2], Teng Li[1, 2], Chong Liu[1, 2], Yufang Ye[1, 2], Xi Zhao[1, 2]

[1]School of Geospatial Engineering and Science, Sun Yat-sen University, Guangzhou, China
[2]Southern Marine Science and Engineering Guangdong Laboratory and the Key Laboratory of Comprehensive Observation of Polar Environment, Ministry of Education, Sun Yat-sen University, Zhuhai, China

Correspondence to: Xiao Cheng (chengxiao9@mail.sysu.edu.cn)

Table S1. Additive 19 images with two types of features added to the training or validation data list

#	Scene names	features	Training or validation list	Repeat times
1	20180108T184332_dmi_prep.nc	highly winded water	training	4
2	20180923T201918_dmi_prep.nc	highly winded water	training	4
3	20180929T081203_dmi_prep.nc	highly winded water	training	4
4	20181022T180429_dmi_prep.nc	highly winded water	training	4
5	20190228T214134_cis_prep.nc	highly winded water	training	4
6	20190308T101217_cis_prep.nc	level thin ice	training	8
7	20190411T205511_dmi_prep.nc	level thin ice	training	8
8	20190519T194808_dmi_prep.nc	highly winded water	training	4
9	20190525T203543_dmi_prep.nc	highly winded water	training, validation	4
10	20190730T123155_cis_prep.nc	level thin ice	training, validation	8
11	20190807T104254_cis_prep.nc	highly winded water	training	4
12	20191201T205227_dmi_prep.nc	highly winded water	training	4
13	20200514T104800_dmi_prep.nc	level thin ice	training	8
14	20200910T194821_dmi_prep.nc	highly winded water	training	4
15	20201029T193925_dmi_prep.nc	highly winded water	training, validation	4
16	20210205T214147_cis_prep.nc	level thin ice	training	8
17	20210220T082107_dmi_prep.nc	level thin ice	training	8
18	20210624T074828_dmi_prep.nc	level thin ice	training	8
19	20211023T194827_dmi_prep.nc	highly winded water	training	4

Figure S1 presents the analysis for 13 Harallick texture features (Haralick et al., 1973). Firstly, (b) shows that the highest J-M distance (Bruzzone et al., 1995) values occur in the 1, 3, and 6 (i.e., HV Cont, HV Var, HV Sum Var) textures, which are consistent with the experiment in (c) that three textures all have good separation ability for different ice types. Referring the example visualization in (a), the 1, 3, and 6 textures tend to highlight bright ice pixels as distinguishable whereas compress the low backscatter surfaces as dark areas. High correlation happens within the 1, 3, and 6 textures. Based on experience from previous studies (e.g., the Table 1 in (Guo et al., 2023)), we selected the 1-HV Cont texture. Additionally, both (a) and (c) indicate that HV Sum Avg provides the clearest ice type segmentation. Sum Avg respects the window-mean backscatter image, an essential basis for sea ice classification. Therefore, HV Sum Avg and HV Cont, as well as the similar HH Sum Avg and HH Cont textures were finally selected.

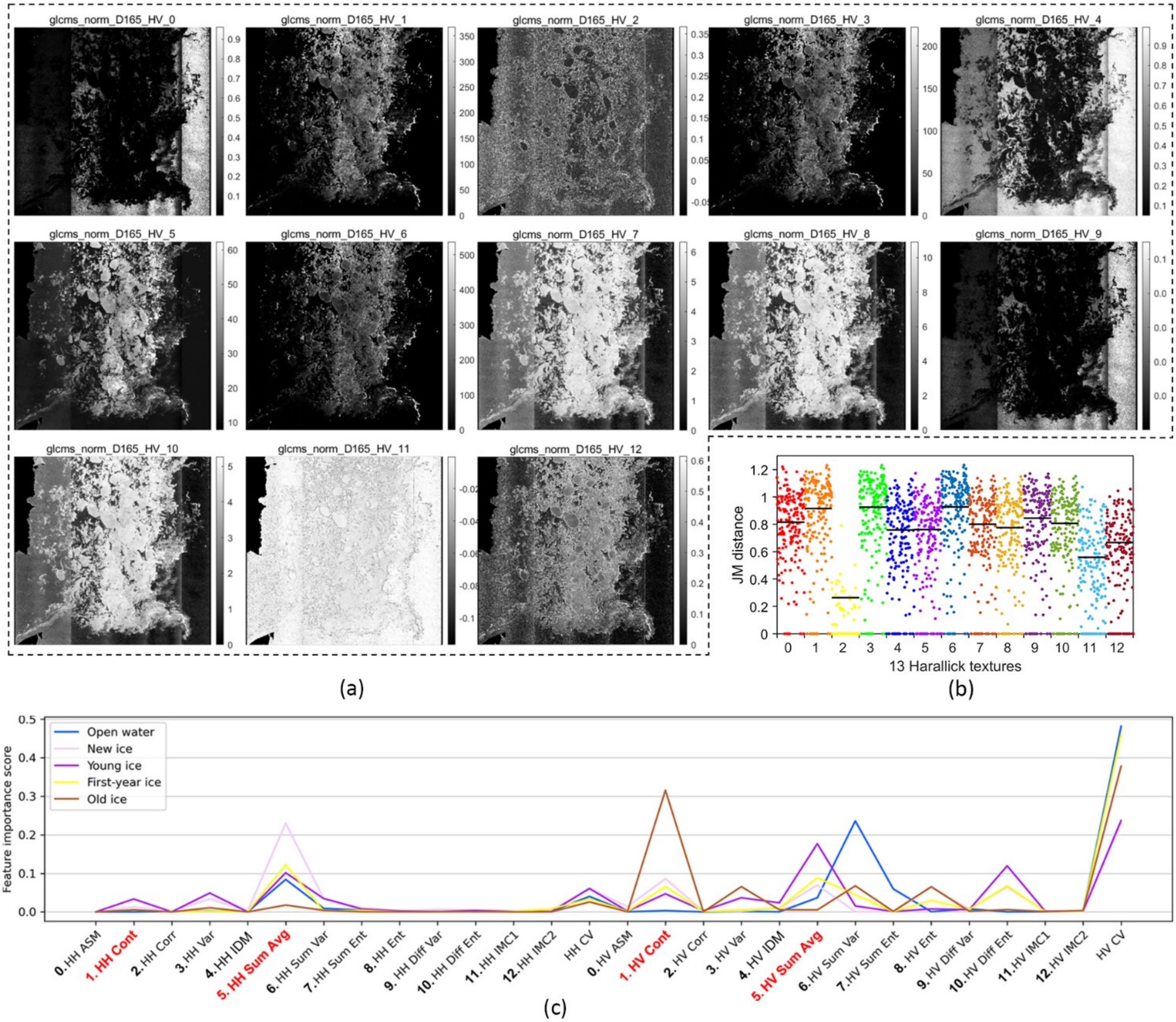

Figure S1. (a) the 13 Harallick textures of one image calculated using the codes from https://github.com/ nansencenter/MOIRA, which is consistent with the texture computation in (Park et al., 2020). The image was acquired on Aug. 19, 2019. (b) shows the scattered J-M distances of 13 Harallick textures calculated between the U-Net predicted ice and water pixels in the 182 SAR HV images. Here, the black level short-lines are the non-zero average J-M distances. (c) shows the feature importance of the binary sub-classifiers, referenced from (Park et al., 2020) under the Creative Commons Attribution 4.0 License that is accessible on https://www.the-cryosphere.net/policies/ licence_and_copyright.html. 4 textures are selected and marked as the red fonts in (c).

30 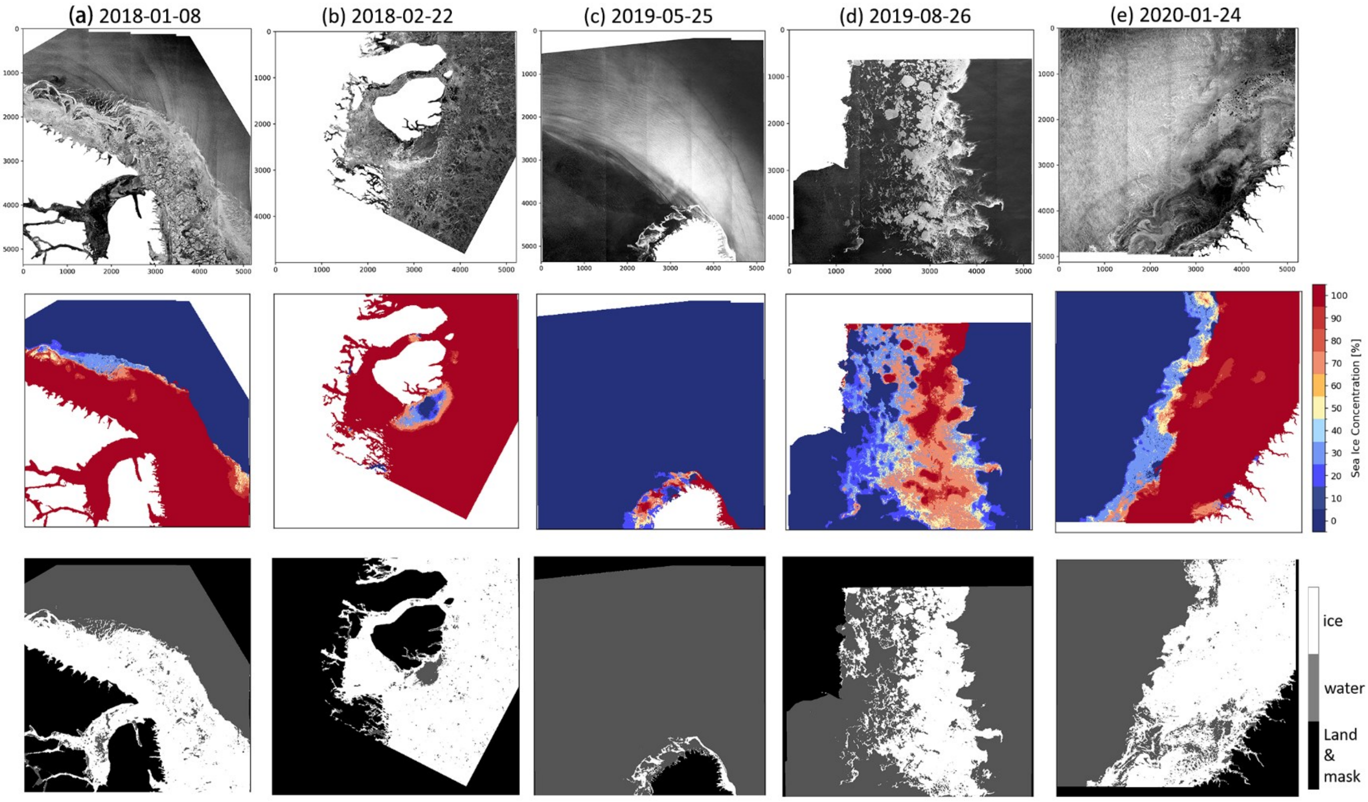

Figure S2. Another five examples with different ice conditions. The first row shows the individual Sentinel-1 SAR HV grayscale images, the second row shows the U-Net predicted SIC maps from which ≥30% SIC is used to segment major ice regions, the third row shows the Multi-textRG algorithm detected ice extent. In the figures, the U-Net model achieved to distinguish semantic ice regions from winded open water with high accuracy and the Multi-textRG algorithm further achieved to extract ice pixel details under varied ice conditions.

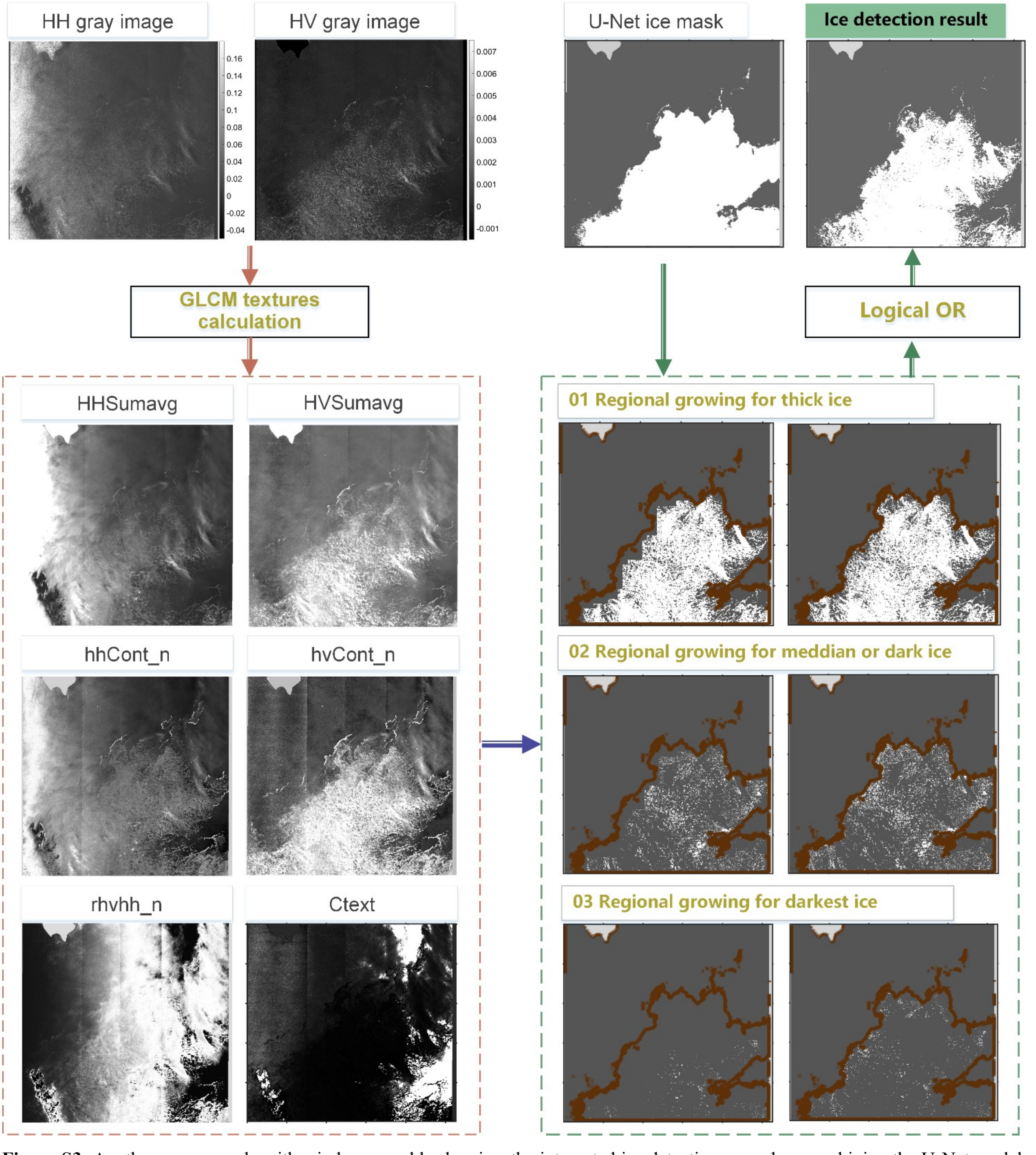

Figure S3. Another one example with winds covered broken ice, the integrated ice detection procedure combining the U-Net model with the Multi-textRG algorithm.

References

Bruzzone, L., Roli, F., and Serpico, S. B., An extension of the Jeffreys-Matusita distance to multiclass cases for feature selection, Ieee T. Geosci. Remote, 33, 1318-1321, doi: 10.1109/36.477187, 1995.

Guo, W., Itkin, P., Singha, S., Doulgeris, A. P., Johansson, M., and Spreen, G., Sea ice classification of TerraSAR-X ScanSAR images for the MOSAiC expedition incorporating per-class incidence angle dependency of image texture, The Cryosphere, 17, 1279-1297, doi: 10.5194/tc-17-1279-2023, 2023.

Haralick, R. M., Shanmugam, K., and Dinstein, I., Textural Features for Image Classification, IEEE Transactions on Systems, Man, and Cybernetics, SMC-3, 610-621, doi: 10.1109/TSMC.1973.4309314, 1973.

Park, J.-W., Korosov, A. A., Babiker, M., Won, J.-S., Hansen, M. W., and Kim, H.-C., Classification of sea ice types in Sentinel-1 synthetic aperture radar images, The Cryosphere, 14, 2629-2645, doi: 10.5194/tc-14-2629-2020, 2020.